Distributed Blade Control

W.P. Engels

S.K. Kanev

T.G. van Engelen

Project UpWind

Contract No.:
019945 (SES6)

"Integrated Wind Turbine Design"

Distributed Blade Control

AUTHOR:	Wouter Engels
AFFILIATION:	Energy research Centre of the Netherlands
ADDRESS:	P.O. Box 1, 1755 ZG, Petten, The Netherlands
TEL.:	+31224564542
EMAIL:	engels@ecn.nl
FURTHER AUTHORS:	S. Kanev and T. G. van Engelen
REVIEWER:	F. Savenije
APPROVER:	L. G. J. Janssen

Document Information

DOCUMENT TYPE	Publication
DOCUMENT NAME:	Distributed Blade Control
REVISION:	0
REV.DATE:	04-10-2010
CLASSIFICATION:	R0: General public
STATUS:	Approved

Abstract: This paper was presented at Torque 2010 "The Science of making Torque from Wind" , Heraklion, Greece

Distributed blade control

W. P. Engels
ECN Wind Energy,
P.O. Box 1, 1755ZG Petten,
The Netherlands
engels@ecn.nl

S. Kanev
ECN Wind Energy,
P.O. Box 1, 1755ZG Petten,
The Netherlands
kanev@ecn.nl

T. van Engelen
ECN Wind Energy,
P.O. Box 1, 1755ZG Petten,
The Netherlands
vanengelen@ecn.nl

Abstract

Wind turbine designs are driven by aerodynamic loads on the structure. If loads are reduced, the dimensions of certain parts and the total cost can be reduced. Individual pitch control (IPC) is known to be effective, but a rotor with distributed blade control (DBC), also known as a smart rotor, can achieve more. With DBC the aerodynamic shape of the blade is adapted locally to reduce loads. Such a system can react quicker than IPC and can be tuned to local conditions.

This paper focusses on the combining different sensors with various control structures and shows what reductions in fatigue load can be obtained with DBC within realistic constraints.

A rotor equipped with two control devices on each blade is examined. The resulting controllers are tuned to achieve performance within constraints and their stability is analysed. A linearised model of the Upwind 5MW reference turbine is used. The resulting damage equivalent loads are compared with those for baseline controller and IPC.

This paper confirms that DBC is effective, reducing the damage equivalent loads by up to nearly 50% relative to the baseline controller. That is 18-27% more reduction than IPC can achieve on its own. From the different sensor-controller combinations measuring the in-blade moments near the DBC actuators is found to be less useful than flapwise blade velocities or blade root moments. The best results are obtained when IPC and DBC are used together. The results show that it is also important to examine the effect on other turbine components.

Keywords: wind turbine control, individual pitch control, load reduction, actuator limitations, smart rotor control, distributed control

1 Introduction

The goal of research into wind turbines is to reduce the cost of energy. One way to achieve a lower cost of energy is by reducing the fluctuations of the loads that act on the wind turbine. This allows the use of lighter parts or improves the life-expectancy of parts. The fluctuations can be reduced by using control to adjust the lift of the aerodynamic profile, for instance by changing the angle of attack relative to the wind experienced at each blade or by adjusting the profile itself.

Individual pitch control [10, 23] is one method to reduce the loads on the structure. However, the load reduction one can achieve with individual pitch control (IPC) is limited, because one has to rotate the entire blade. This results in two limitations; on the one hand, the acceleration is limited and on the other, the response is the same along the whole blade. Active devices on the trailing edge that adapt the local aerodynamic shape have been shown to act quick and the response can be tailored to the location and loads along the blade.

Research has mainly focussed on the aerodynamic modelling of the devices that can adjust the aerodynamics, mainly flaps (or deformable trailing edge geometries) [6, 21], tabs [27, 13] or synthetic jets [9]. Flaps have been added to a wind turbine model and were shown to work with a controller in a simulation [19]. Flaps were also built and shown to work well in a non-rotating wind tunnel test [25]. Attention has also gone to where the actuators are most effective [1]. More extensive overviews of recent work were conducted by Barlas and van Kuik [4] and by Berg et al [7].

Across this work, there was relatively discussion on the choice of sensor type and sensor location in combination with the control strategy. This paper compares the performance of different control strategies based on different sensors.

2 Approach

We examine a linearised aeroelastic model of a wind turbine at three different average wind speeds (11, 15 and 20 m/s). A baseline controller is used for rotor speed and power regulation. IPC is also designed to reduce static tilt and yaw rotor moments.

Several combinations of controller structure and sensor type are explored. We examine two ways

of using the sensors and actuators, one uses the sensors and actuators separately on each blade (in rotating coordinates), the other combines the sensor and actuator signals using modulations of the rotational speed. Though the control strategies that are used here are relatively simple, handling the actuator constraints well and proving stability are not trivial; this will be further explained.

3 Model

3.1 Aeroelastic turbine model

A linearised aeroelastic model of the Upwind 5 MW reference turbine [16] is used, which is a slightly modified version of the NREL 5 MW reference turbine [18]. The model is obtained using Turbu [24]. Turbu generates a linear, time-invariant (LTI) model of the wind turbine. The model is linearised at a particular average wind speed and a particular wake-structure. The LTI model allows the application of standard design methods such as LQG, $\mathcal{H}_2$ and $\mathcal{H}_\infty$ and allows stability (margin) assessment. The aerodynamics are based on a BEM model and a total of 14 annuli were assumed, where the first and last are only half as wide as the others.

Realistic wind excitation signals are applied to the blade, representing both stochastic (turbulence) and deterministic (tower shadow, wind shear) effects. More specifically, time-series of wind excitation signals are generated for each blade element. Each signal represents a wind speed realisation along a helix, corresponding with a volume of air passing through that part of the rotor. This helix-based wind modelling approach has the advantage of low computational complexity and while achieving an accurate approximation of the effect of 3D turbulence on the loads of the blade elements [22].

3.2 Baseline and IPC control

The baseline controller is a basic controller consisting of torque control on the basis of a QN-curve and a proportional-integral action (PI) that changes the collective pitch angle to regulate rotor speed. This basic controller is extended with gain-scheduling, notch filters at the tower frequency and drive train frequency, a low pass-filter with 20 dB reduction at 3p and basic transition management of the cross-over region between rated and below-rated production.

An example of more advanced control of torque and pitch angle can be found in [26]

The IPC controller is based on integrator loops acting on the tilt and yaw moments from which the tower, 3p and 6p frequencies are filtered out [10, 23].

Figure 1: The distributed controller uses two actuators on each blade

3.3 Distributed actuator model

The actuator is an active device on the trailing edge that can effectively change the aerodynamic properties of the section of the blade the device is attached to. Because the higher-frequency (aero)dynamics of the devices are not yet explored and because we did not want to limit this study to a particular device, we assume generic, independently controlled actuators that change the local *aerodynamic pitch* of the blade.

We assume there are two of these actuators on each blade. One is located at a radial position of 50% to 73% of the blade length (the inner actuator). The second, adjacent to the first, covers 73% to 88% of the blade length (see Figure 1). The actuators respectively cover 3 and 2 annuli. These locations and lengths have not been optimised, though earlier work [1] indicates a similar range.

The change in aerodynamic lift from a step change in the angle of attack of an aerofoil is not instant and changes over time. These effects are known as unsteady aerofoil aerodynamics and dynamic inflow.

There are various ways of calculating the lift as a function of time after a change in the angle of attack due to the unsteady aerofoil aerodynamics. For a sinusoidally oscillating aerofoil, an approximation of Theodorsen's solution given in [12]:

$$C(k) = 1 - \frac{0.165}{1 - \frac{0.0455}{k}i} - \frac{0.335}{1 - \frac{0.30}{k}i} \qquad (1)$$

where $k = \omega c/2U$, where ω is the frequency of the oscillation, c is the chord of the aerofoil, U is a steady oncoming wind speed and $i = \sqrt{-1}$. The function $C(k)$ is a transfer function in the normalised frequency k, that gives the phase and amplitude relative to a steady ($\omega = 0$) unit change in the angle of attack.

With equation (1), one can calculate a frequency ω for which the amplitude of the response remains within an arbitrary margin of the steady-state response. This could be considered a maximum 'bandwidth' for the controller. If we demand that the amplitude of the response should be at least $1/2\sqrt{2}$ (-3dB) of the steady-state response, the bandwidth of the controller ought not be more than 5.9 rad/s for the innermost edge of the inner actuator, while one could allow 16.1 rad/s for the outermost edge of the outer actuator. The phase-shift

according to this approximation would be 15°.

More detailed analyses concerning the unsteady aerofoil aerodynamics have also been performed for specific actuators, e.g. the effect of variable trailing-edge geometry [21, 2] and microtabs [13]. The effect of synthetic jets is still being investigated [9].

Another way to use equation (1) is to recognise that the approximation indicates that the response is always within the range 0.5-1, even for high-frequencies. That means that if we demand that the amplitude of the response is at least 0.5 of the steady-state response, the allowed 'bandwidth' is infinite. One could therefore also consider unsteady aerofoil aerodynamics to be an uncertainty in the control gain and phase.

The dynamic inflow effect of the use of the actuators has been taken into account, as described in [22], although for frequencies that are multiples of the rotational frequency, this is not expected to make a significant difference.

The actuators will also have some dynamics, but these depend on the type of actuator one chooses to use. Both the effect of the unsteady aerodynamics and the actuator dynamics, could possibly be compensated for if one uses an inverse model to drive them.

Here unsteady aerodynamics and actuator dynamics have been ignored, but the response of the distributed controllers is limited both in amplitude and velocity.

3.4 Constraints

Both the blade pitch mechanism and the distributed control actuators have physical constraints. We have a assumed a maximum pitch speed of 8°/s and a maximum pitch acceleration of 16°/s².

For the distributed controller it is impossible to establish constraints without assuming properties of a specific device. Most studies investigating control have so far used flaps; Lackner [19] and Barlas [5] assume 10% chord length actuators that can achieve a maximum deflection of 10° and a maximum speed of 40°/s. Berg et al. [8] assume 20° and 100°/s respectively, while Andersen et al. [1] assume a 5° maximum deflection. Troldborg [21] showed that turning a curved flap of 10% of the chordlength through one unit angle, approximately corresponds to turning the entire aerofoil 42-45% of one unit angle (depending on the flap geometry).

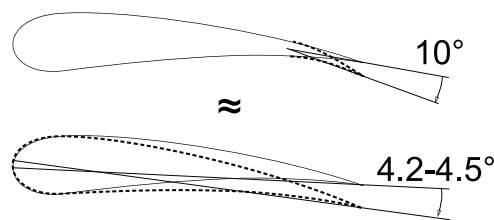Here we have assumed a maximum rotation of the aerofoil of ±5°. For the rate of change in aerofoil

Figure 2: Turning a 10% chord length, curved flap 10° corresponds to turning the profile 4.2-4.5° [21]

angle a maximum velocity of 20°/s is assumed.

4 Distributed controller design

There are multiple controllers for blade load reduction using active devices on the blades that have already been explored. These include proportional (P) and proportional-derivative (PD) control based on flapwise blade [1] or tip deflections [8], PID control based on the tilt and yaw components of the blade root moment [19] and a smoothed PD with an additional notch filter based on the blade root moments in a fixed, non-rotating set-up [25]. From a control point of view, that leaves a great many options open for exploration.

For distributed control strategies, where sensors and actuators are used over a large part of the structure, it is important to decide whether to use a centralised or a decentralised controller. A centralised controller uses all sensors signals to calculate the control action of each actuator. A decentralised controller decides the control action of an actuator using the measurement of a single sensor (multiple single-input-single-output controllers). Centralised controllers have the advantage that they can achieve better performance, because they have more information available, whereas decentralised controllers tend to require less computational effort, no centralised architecture and can be very robustly stable if one of the sensors or actuators fails.

The controllers that have been examined so far are either decentralised controllers or they act on the Coleman transform [14] of the sensor and actuator signals. The transform allows the rotor tilt and yaw components to be acted on as though they were separate sensors and separate controllers. This could be considered to be somewhere in between a fully decentralised set-up and a fully centralised controller.

An example of a fully centralised controller would be the application of an linear quadratic Gaussian (LQG) controller to the Coleman transformed model. An LQG controller consists of a linear quadratic regulator (LQR), a gain matrix that calculates the response on the basis of the states and a Kalman filter for that estimates those states.

frame	controller structure	velocity	in-blade bending moment	blade root moment
rotating	filtered P	X	X	X
rotating	IMP	X	X	X
1p mod	filtered I		X	X
1p mod	IMP		X	X
np mod	filtered I			X

Table 1: Explored controller structure and sensor combinations

Here an array of possible control sensors and controller structures was analysed under equal circumstances. The combinations we examined are indicated in Table 1 (options and combinations are further explained below). Fully centralised controllers are not examined.

4.1 Sensors

The sensor signals we examined are the flatwise blade velocities at the centre of each actuator (at 62% and 81% of the blade radius), the in-blade bending moments at the innermost part of each actuator (at 50% and 73% blade radius) and the blade-root-moments.

4.2 Controller structure

The controller structure was also varied. We examined controller structures based on simple filters, the internal model principle (IMP) and a controller based on modulations at multiples of the rotational frequency (np-modulated)

4.2.1 Filtered controllers

For the signals in the rotating domain, one basic structure is a filtered proportional (P) controller. The filters consist of real-valued poles and zeros for which the location was part of a controller optimisation. This is further discussed in section 4.4. The option of absolute velocity feedback in combination with filters is examined a bit more in depth.

For the 1p-rotationally modulated signals, the controller is a filtered integral (I) controller. For these signals, the filter consists of band-stop filters at multiples of the blade-pass frequency, i.e. at 3p,6p,9p,..., depending on what is appropriate at that particular modulation.

Skyhook control
Proportional absolute velocity feedback is also known as skyhook-damping and is a well known concept in the field of active vibration control (e.g [3]). For further reading in the field of active vibration control, the reader is referred to [15, 20].

With skyhook-damping, the absolute velocity at a point on a structure is measured and an actuator is used to generate a force that is proportional but in opposite direction to the measured velocity. If the

sensor and actuator are co-located this is a very robust control approach, because the sensor and actuator can only absorb energy. It is equivalent to a damper attached to a non-moving coordinate system (hence the name sky-hook damping).

If we differentiate or integrate the velocity signal to obtain acceleration or position feedback and use that for control, we get control structures that are equivalent to added mass (acceleration feedback) or a skyhook stiffness (position feedback). Because these are all 'passive' control strategies, (i.e. they cannot add energy to the system) that also means that if multiple of such loops are applied to a structure, they must all remain stable (assuming we have ideal sensors and actuators and no delays).

In our model, the control action corresponds to a local change in the aerodynamic pitch of the blade. This results in a change of the lift and drag forces on that section of the blade, with the largest change in the flat-wise direction. To make sure the control force and the measured velocity act along the same axis, we have used the velocity of the blade in flat-wise direction. It is difficult to measure the true absolute velocity, but a common approximation is the integrated signal of an accelerometer. This might give some drift problems at very low frequencies, on the other hand, very low frequency ($\ll$1p) changes in the loads represent changes in the rotor-average wind and ought to be taken care of by the baseline controller. This means that the drift problem can be solved using a high-pass filter at a low frequency.

Because we used multiple poles, the filter can not be considered completely equivalent to a damper, mass or stiffness and the 'passiveness' of the controller is not guaranteed. A Coleman transform of the filters at the selected operating point was combined with the linearised model to verify analytically that the controller remains stable (see appendix A).

4.2.2 IMP

Another structure is based on the internal model principle (IMP). In this case the model that is assumed is a representation of the main load components at the rotational frequencies.

For the control in rotating coordinates, the IMP controller consists of a combination of inverse-notch filters at multiples of the rotational frequencies p. Each of these subfilters consisted of a real valued zero and 2 complex-valued poles. The frequency of the poles is kept at 1p,2p,3p depending on the subfilter. The optimisation is allowed to vary the damping of the poles (i.e. the Q-factor of the filter), the location of the real-valued zero and the
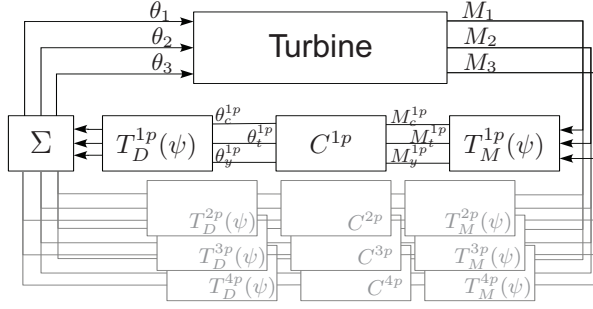
Figure 3: Structure of mmDBC

gain of each filter.

The combination of IMP control with velocity feedback is similar to the use of tunable vibration absorbers (e.g. [11]). Tunable vibration absorbers are commonly used to target specific excitation or structural frequencies.

For the Coleman transformed sensor signals, the IMP controller structure is targeted at the asymmetric rotor loads (tilt and yaw rotor loads) at the frequencies 0 and 3p in fixed frame, equivalent to 1p, 2p and 4p frequencies on the rotating blade (3p blade flapping is symmetric, and can be controlled using the axial component of the Coleman transformed signals). According to the internal model principle, in order to completely reduce 0p and 3p loads on the rotor, the controller should consist of an interconnection of an integrator and an inverse notch at the 3p frequency. In practice, since the rotational frequency of the rotor varies, the notch is substituted by a lightly damped second order filter, resulting in the following IMP controller structure:

$$
C_{IMP}(s) = \underbrace{G_0 \frac{1}{s} F_0(s)}_{\text{0p control}} + \underbrace{G_3 \frac{2c(3p)s}{s^2 + 2c(3p) + (3p)^2} F_3(s)}_{\text{3p control}}
$$

(2)

where $F_0(s)$ and $F_3(s)$ are suitable filters, and 2-by-2 gain matrices $G_0(s)$ and $G_3(s)$ are computed by using static output H_∞ optimization.

The IMP controller is designed for a model in the fixed reference frame, and hence has the advantage that the wind turbine model is time-invariant, i.e. it does not depend on the azimuth angle. This allows the use of advanced controller design techniques for linear systems with guaranteed closed-loop stability. A disadvantage of this controller structure is that actuator constraints cannot be explicitly appropriately handled due to the 3p band-pass filter in the controller.

4.2.3 Multi-rotational modulated control (mmDBC)

The idea behind multi-rotational modulated control (mmDBC) is to use a set of coordinate transformations to transform the blade flapwise loads at frequencies multiple of the rotational frequency (1p,

2p, 3p, etc.) to static loads in other coordinate systems [23]. These coordinate transformations are referred to here as multi-rotational modulations. An np-modulation, n=1,2,3,..., transforms the blade bending moments M_1, M_2, M_3 at and around the np frequency to quasi-static loads $M_c^{np}, M_t^{np}, M_y^{np}$. These loads can then be reduced by using simple integrator-based control structures. The outputs of these controllers $\theta_c^{np}, \theta_t^{np}, \theta_y^{np}$ need to be transformed back to the original blade coordinates and are added up for the various modulations to create the desired angles for the actuators on the blades (see Figure 3).

In contrast to the IMP approach, where the control structure involves narrow band pass filters at the frequencies at which reduction is required, the mmDBC approach results in integral control structures that significantly simplify the implementation of schemes for dealing with actuator limitations (anti-windup schemes). A method for translating the original constraints of the distributed control devices to constraints in the np-modulated coordinate systems has been developed. The method distributes the available actuation freedom betweeen the different control loops (see Figure 3) according to the required control activity in each loop.

A disadvantage, on the other hand, is that the wind turbine model in these transformed coordinates is dependent on the azimuth angle[1], which makes the application of linear controller design and analysis tools not directly possible.

The azimuth dependency introduces parasitic 3p and 6p effects on the outputs of the model, but these can effectively be notched out in the controller, resulting in an input-output behaviour that can well be approximated with a linear time-invariant model. One way to construct this approximate linear model is by using system identification methods on input-output data obtained by simulating the np-modulated model with low frequency excitation (with a bandwidth of, say, 0.1 Hz) on the inputs $\theta_c^{(np)}, \theta_t^{(np)}, \theta_y^{(np)}$.

4.3 Stability analysis

We use different methods to establish stability, depending on the control strategy. For controllers that use measurements in the rotating domain, it was realised that they could be Coleman-transformed to a linear controller in the non-rotating coordinates (see appendix A). Combined with the linear wind turbine model this results in a linear model that can be analysed with linear methods. The controllers

---

[1]Exception is the 1p-modulation, also called Coleman transformation, that results in azimuth independent linear time-invariant model.

based on the Coleman transform are already in an LTI format.

For the multi-rotational modulated controllers, a Floquet analysis is used to establish stability. Such an analysis is described for instance by [17].

Both the Floquet analysis and the Coleman transform are limited in their validity by the assumption of a constant rotor speed and linear base-line control. Therefore the time-series of the controller signals from the distributed controllers were also examined.

To establish robustness, additional simulations were done where the gains and the delays of the actuators on the blades were varied independently. Because of the different gains for the actuators, the blades are no longer equal and a Coleman-transform of the controller will not yield a time-invariant linear model. Therefore the time-series were examined. With gains varying between 0.5 and 2 times their original value and delays up to 0.1 second, the time-series showed no sign of instability.

4.4 Optimisation

For the filtered and IMP controllers in rotating co-ordinates, an optimization program is used to select the filter gains and pole and zero locations. The optimization algorithm is a localised random search for the parameters that are allowed to vary. The results can therefore only be guaranteed to be locally, but not globally, optimal. The algorithm optimized the variables to obtain a minimum design equivalent load on the flatwise blade root moment, while making sure that the controller remained stable and that its output did not exceed the actuator constraints in a 500 second simulation.

The optimisation of the filters occurred on a linearised model with a linearised baseline control and individual pitch control at an average wind speed of 15 m/s.

As expected, it appeared in the optimisation that the constraints of maximum amplitude and speed of the actuator, rather than the stability constraint, resulted in limited gains of the distributed controller.

5 Results

It would not be practical to discuss all examined controllers here. We will limit ourselves to the two combinations that gave the best results: rotating, filtered velocity feedback ('skyhook') and multi-rotational modulated, filtered integral feedback (mmDBC) of the blade root moments.
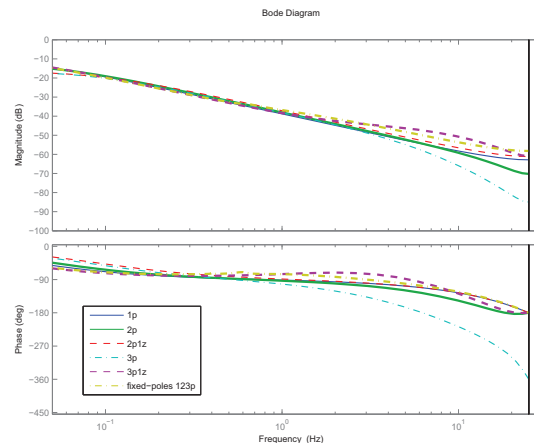

Figure 4: Controllers with optimised filters for velocity feedback at the outer actuator location show similar response

5.1 Resulting velocity feedback controllers

Figure 4 shows the bode response of the resulting (decentralised) controllers for the outer actuator. These controllers are all based on velocity feedback in the rotating frame, but have varying structures.

The structures used are proportional controllers with filters consisting of 1 pole (1p), 2 poles (2p), 2 poles and 1 zero (2p1z), 3 poles (3p) and 3 poles and 1 zero (3p1z). These 'p's denote the number of poles, not multiples of the rotational frequency of the turbine. The figure also shows the optimised result of a controller based on an IMP controller aimed at 1, 2 and 3p.

The response of each of these optimised controllers shows a very similar trend, in the frequency region depicted, i.e. a 20 db/decade declining amplitude and a 90 degree phase shift. At low frequencies the response is constant. This effectively corresponds to the response of a first order low-frequency high-pass filter, applied to an integral controller. This control applied to a velocity feedback signal is similar to proportional displacement feedback combined with a high-pass filter. This is similar to some of the controllers used in earlier publications ([1, 8]). In combination with the velocity feedback controller, the filter with 2 poles performed best. One of these poles was located at a low-frequency, the other at high frequencies.

5.2 Simulation results

We examined the effectiveness of the controllers at three different wind-speeds, i.e. 11, 15 and 20 m/s. At 11 m/s we used the non-linear baseline controller as described in section 3.2. At 15 and 20 m/s we used linearised versions of the controller, without gain-scheduling. Some time-lag was in-
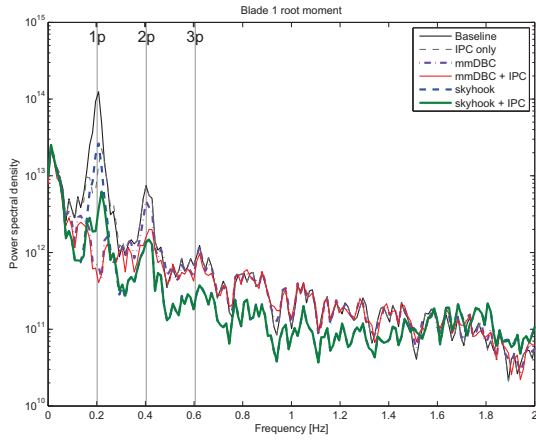
Figure 5: Spectrum for 15 m/s wind with distributed control options

Figure 6: Power production and pitch angle in a simulation with 11 m/s wind, with distributed control options

cluded in the simulation, to prevent instant feedback in the system. In the simulations, we have not adjusted any of the parameters of the distributed controllers as a function of the rotor or wind speed.

The design equivalent loads are calculated for a composite material with a fatigue exponent of 10 for one timeseries of 500 seconds at each windspeed. As a measure of the control effort, the root-mean-squared (RMS) of the pitching velocity of the blade as a whole and the distributed actuators are also investigated. These are shown in Table 2.

The results show that a reduction of the design equivalent load of up to 47% is possible.

Figure 5 shows the spectrum of the flatwise blade root moment loads for various control options. The skyhook controller is actively reducing the loads over a much wider part of the spectrum. At 2 Hz, there does seem to be some amplification of the loads. The mmDBC controller mainly achieves its reduction at 1 and 2p and achieves a significantly higher reduction at 1p than the skyhook controller.

Figure 6 shows a time-series of power and pitch angle for the non-linear controller with 11 m/s average wind. The figures show that there is no significant change in power production relative to the baseline controller, but do show that the pitching with the mmDBC controller is less than for skyhook control.

Figures 7a and 7b show pitch angle of the distributed actuators on the blade and the blade root moment of one of the blades for part of this timeseries. It shows that skyhook and mmDBC both reduce the variation of the loads, but with different control actions. Smart rotor control also affects tower motion. Table 3 shows the 'design equivalent translations' (a rainflow count of the displacements) of the tower top. Skyhook control can de-
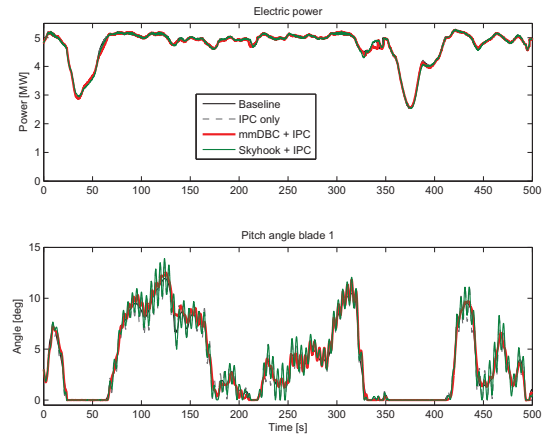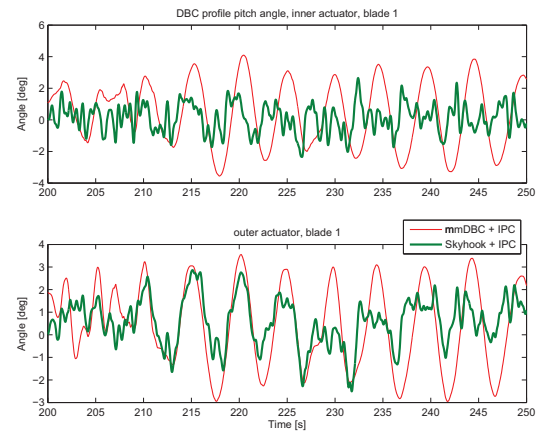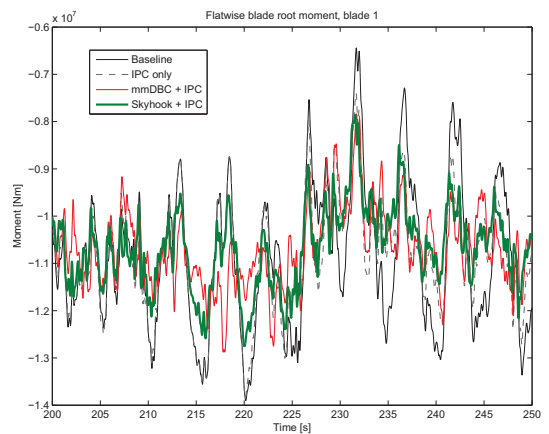

(a) Distributed pitch angle

(b) Blade root moments

Figure 7: Results for part of the time series of a simulation with 11 m/s wind, with distributed control options

crease the motions in both fore-aft and side-to-side motion. mmDBC on the other hand, tends to have an overall detrimental effe ct on the motions. This may be amended with extra notch filters.

A side effect of employing skyhook control is that the gain margin for the individual pitch controller is increased. Initial investigations show that optimising the optimal velocity feedback in combination with individual pitch control allows for even more reduction in the design equivalent load. This is mostly due to extra suppression of the 1p component in the loads. It can be expected that mmDBC, which already suppresses this frequency very effectively, will benefit less.

6 Conclusions, discussion, future work

We examined different combinations of controller structures and sensor signals for reducing the flatwise blade root moments. The most effective of these were absolute velocity feedback (skyhook) with a filter that is similar to an integrator in combination with a high-pass filter and a non-linear controller based on modulation of the blade root moments at multiples of the rotational frequency (1p,2p,3p) (mmDBC).

The results show that distributed control within the chosen constraints can reduce the blade root moment significantly: nearly 50% in design equivalent load.

We saw that the multi-rotational modulated control was considerably better at reducing the 1p loads than that the skyhook controller and resulted in significantly reduced efforts for blade pitching. The skyhook controller, on the other hand, showed overall better performance and reduced loads over a wider frequency range.

A significant reduction of the tower-top motions, both fore-aft and side-to-side, was observed for skyhook control, but applying mmDBC resulted in an increase. This shows it is important to look at more variables than just the one being minimised. To improve the result for mmDBC either a notch filter can be included or an extra loop for tower damping can be added.

An absolute velocity feedback controller combined with an integrator is similar to a proportional displacement feedback controller. We already discussed that others also used proportional displacement feedback controllers, ([1] and [8]). Andersen et al. remark on the use of the PD controller for displacement feedback: *Using a PD regulator instead of a P regulator will make the flaps roughly twice as efficient.* The efficiency meant here is the amount of reduction for a unit of effort of the actu-

ators. A PD controller for displacement feedback is equivalent to an integral controller for velocity feedback with a significant proportional component at high frequencies. The controllers that we found showed no significant proportional part at high frequencies, while the controller structure did allow for it.

There can be several causes for this difference, first of all, the controllers we examined were selected on maximum performance within the actuator limitations, the controller designed by Andersen et al. was designed for maximum performance at a particular control effort. Other causes of the difference could be the different constraints on the controller or the inclusion of a different time lag in this study.

If one uses IPC and/or distributed blade control for load alleviation this ought to result in lower induction in parts of the swept area with higher wind and higher induction for parts with lower wind speeds. Especially for situations with strong wind shear, with an average wind below rated this could affect the wake structure. This might also result in power loss. For the wind speeds we examined, even at slightly above rated wind speeds, no power loss was observed.

Acoustic noise can also be affected. Noise is assumed to be caused by the turbulence in the boundary layer and the volume of the noise is assumed to affected by the thickness of the boundary layer. The thickness of the boundary layer is affected by the camber, but could also be affected by the motion of the wind turbine blade.

Future work
Despite the encouraging results there is still much to be examined, both in a wider context of the entire turbine and specifically for the controllers that are designed for distributed blade control.

Further research should include:
○ non-linear simulation of the wind turbine
○ an examination of how distributed blade controllers affect extreme loads.
○ a study where a dynamic model of the change in lift as function of time is and a dynamic model of the actuators is included that also examines whether these dynamics can be compensated for using inverse models. An analysis on the aerodynamic limitations due to non-linearity and stall should be included.
○ a study examining how velocity, position and effort constraints affect controller design and maximum obtainable performance
○ a strategy for below-rated operation should be further examined, minimising noise and loads and maximising power are likely to require con-

flicting actions.

○ a comparison of the decentralised control strategy and a LQG controller applied to the Coleman transformed model should be examined to establish how the performance of these controllers compare.

○ it should be examined whether a combination of multi-rotational modulated *individual pitch control* and velocity feedback control results in even better performance.

○ the reduction of the tower-top-motions observed for skyhook control may benefit the stability of the individual pitch controller and baseline controller. It should be examined whether the notch filters that are employed now to filter out some of these motions are still needed in combination with distributed blade control.

○ a study aimed at the effects on the design equivalent loads of other parts of the wind turbine (mainly hub, nacelle frame and tower)

○ an optimisation of the choice of location, length and number of devices in combination with varying control strategies to confirm the results presented in [1].

Acknowledgement

References

[1] Peter Bjørn Andersen, Mac Gaunaa, Christian Bak, and Thomas Buhl. Load alleviation on wind turbine blades using variable airfoil geometry. In *Proceedings of the European Wind Energy Conference and Exhibition (EWEC)*, 2006.

[2] Peter Bjørn Andersen, Mac Gaunaa, Christian Bak, and Morten Harvig Hansen. A dynamic stall model for airfoils with deformable trailing edges. *Journal of Physics: Conference Series The Science of Making Torque from Wind*, 75, 2007.

[3] M. J. Balas. Direct velocity feedback control of large space structures. *Journal of Guidance and Control*, 2(3):252–253, 1979.

[4] T. K. Barlas and G. A. M. van Kuik. State of the art and prospectives of smart rotor control for wind turbines. In *The Science of Making Torque from Wind*, 2007.

[5] T. K. Barlas and G. A. M. van Kuik. Aeroelastic modelling and comparison of advanced active flap control concepts for load reduction on the upwind 5mw wind turbine. In *Proceedings of the European Wind Energy Conference and Exhibition (EWEC)*, 2009.

[6] Santiago Basualdo. Load alleviation on wind turbine blades using variable airfoil geometry. *Wind Engineering*, 29(2):169–182, 2005.

[7] Dale Berg, Scott J. Johnson, and C. P. van Dam. Active load control techniques for wind turbines. Technical Report SAND2008-4809, Sandia National Laboratories, 2008.

[8] Dale E. Berg, David G. Wilson, Matthew F. Barone, Brian R. Resor, Jonathan C. Berg, Joshua A. Paquette, Jose R. Zayas, Shridhar Kota, Gregory Ervin, and Dragan Maric. The impact of active aerodynamic load control on fatigue and energy capture at low wind speed sites. In *Proceedings of the European Wind Energy Conference and Exhibition (EWEC)*, 2009.

[9] C. S. Boeije, H. de Vries, I. Cleine, E. van Emden, G. G. M. Zwart, H. Stobbe, A. Hirschberg, and H. W. M. Hoeijmakers. Fluidic load control for wind turbine blades. In *47th AIAA Aerospace Sciences Meeting Including The New Horizons Forum and Aerospace Exposition, January*, 2009.

[10] E.A. Bossanyi. Individual blase pitch control for load reduction. *Wind Energy*, 6:119–128, 2003.

[11] M. J. Brennan and J. Dayou. Global control of vibration using a tunable vibration neutralizer. *Journal of Sound and Vibration*, 232(3):585–600, May 2000.

[12] Tony Burton, David Sharpe, Nick Jenkins, and Ervin Bossanyi. *Wind Energy Handbook*. Wiley, 2001.

[13] Raymond Chow and C.P. van Dam. Unsteady computational investigations of deploying load control microtabs. In *44th AIAA Aerospace Sciences Meeting and Exhibit, Reno, Nevada, Jan. 8-11,2006*, 2006.

[14] Robert P. Coleman. Theory of self-excited mechanical oscillations of hinged rotor blades. Technical Report NACA-ARR-3G29, NASA, 1943.

[15] C. R. Fuller, S. J. Elliott, and P. A. Nelson. *Active Control of Vibration*. Academic Press, London, 1996.

[16] H.B. Hendriks, P.J. van Langen, and et al. Upwind reference wind turbine version 008.xls. Excel sheet (internal communication), February 16 2007.

[17] Johnson. *Helicopter theory*. Princeton University Press, 1980.

[18] J. Jonkman, S. Butterfield, W. Musial, and G. Scott. Definition of a 5-mw reference wind turbine for offshore system development. Technical Report NREL/TP-500-38060, NREL, February 2009.

[19] Matthew A. Lackner and Gijs van Kuik. A comparison of smart rotor control approaches using trailing edge flaps and individual pitch

control. *Wind Energy*, published online July 2009 2009.

[20] André Preumont. *Vibration Control of Active Structures: An Introduction*. Kluwer Academic Publishers, second edition, 2002.

[21] Niels Troldborg. Computational study of the Risø-b1-18 airfoil with a hinged flap providing variable trailing edge geometry. *Wind Engineering*, 29:89–113, 2005.

[22] E. L. van der Hooft, T. G. van Engelen, J. T. G. Pierik, and P. Schaak. Real-time process simulator for evaluation of wind turbine control systems. Technical Report ECN-E-07-046, ECN, 2007.

[23] T. G. van Engelen. Design model and load reduction assessment for multi-rotational mode individual pitch control (higher harmonics control). In *Proceedings of the European Wind Energy Conference and Exhibition (EWEC)*, 2006.

[24] T. G. van Engelen and H. Braam. Turbu offshore, computer porgram for frequency domain analysis of horizontal axis offshore wind turbines; implementation. Technical Report ECN-C-04-079, ECN, 2004.

[25] J. W. van Wingerden, A. W. Hulskamp, T. Barlas, B. Marrant, G. A. M. van Kuik, D.-P. Molenaar, and M. Verhaegen. On the proof of concept of a 'smart' wind tubine rotor blade for load alleviation. *Wind Energy*, 11:265–280, 2008.

[26] D.A.J. Wouters and T.G. van Engelen. Modern wind turbine controller design. Technical Report ECN-M–08-060, ECN, 2008. Presented at the Global Wind Power 2008, China Wind Power 2008, Beijing, China, 29-31 oktober 2008.

[27] J. R. Zayas, C. P. van Dam, R. Chow, J. P. Baker, and E. A. Mayda. Active aerodynamic load control for wind turbine blades. In *Proceedings of the European Wind Energy Conference and Exhibition (EWEC)*, 2006.

A Coleman transform of isotropic state space matrices

We want to show that controllers acting on local signals on the rotor result in a stable system. A practical way of doing so is Coleman transforming the control strategies to the 'fixed frame', Coleman domain and combining that with the Coleman transformed model of the wind turbine.

Let's assume we have the filters of the control functions of each blade organised in a state space system:

$$\dot{\mathbf{x}} = \mathbf{A}\mathbf{x} + \mathbf{B}\mathbf{u} \quad (3)$$

$$\mathbf{y} = \mathbf{C}\mathbf{x} + \mathbf{D}\mathbf{u} \quad (4)$$

where $\mathbf{x}$ are the states of the filter, $\mathbf{u}$ is the input and $\mathbf{y}$ is the control function.

A.1 Applying a general coordinate transformation

We wish change the states to Coleman transformed states by applying[3]:

$$\mathbf{x}_{cm} = \mathbf{C}_{cm}^{-1}\mathbf{x} \quad (5)$$

and we want a new set of statespace equations like 3 and 4, where $\dot{\mathbf{x}}_{cm}$ depends on $\mathbf{x}_{cm}$. Starting at equation (5):

$$
\begin{aligned}
\dot{\mathbf{x}}_{cm} &= \left(\dot{\mathbf{C}_{cm}^{-1}}\right)\mathbf{x} + \mathbf{C}_{cm}^{-1}\dot{\mathbf{x}} \\
&= \left(\dot{\mathbf{C}_{cm}^{-1}}\right)\mathbf{C}_{cm}\mathbf{x}_{cm} + \mathbf{C}_{cm}^{-1}\left(\mathbf{A}\mathbf{x} + \mathbf{B}\mathbf{u}\right) \\
&= \left(\dot{\mathbf{C}_{cm}^{-1}}\right)\mathbf{C}_{cm}\mathbf{x}_{cm} + \mathbf{C}_{cm}^{-1}\mathbf{A}\mathbf{C}_{cm}\mathbf{x}_{cm} + \mathbf{C}_{cm}^{-1}\mathbf{B}\mathbf{u} \\
&= \left(\left(\dot{\mathbf{C}_{cm}^{-1}}\right)\mathbf{C}_{cm} + \mathbf{C}_{cm}^{-1}\mathbf{A}\mathbf{C}_{cm}\right)\mathbf{x}_{cm} + \mathbf{C}_{cm}^{-1}\mathbf{B}\mathbf{u}
\end{aligned}
$$
$$(6)$$

We have used the fact that equation (5) implies $\mathbf{x} = \mathbf{C}_{cm}\mathbf{x}_{cm}$ to get rid of terms containing $\mathbf{x}$.

We will also want our in- and outputs as Coleman Coordinates. Thus equation (6) becomes:

$$
\begin{aligned}
\dot{\mathbf{x}}_{cm} &= \left(\left(\dot{\mathbf{C}_{cm}^{-1}}\right)\mathbf{C}_{cm} + \mathbf{C}_{cm}^{-1}\mathbf{A}\mathbf{C}_{cm}\right)\mathbf{x}_{cm} \\
&\quad + \mathbf{C}_{cm}^{-1}\mathbf{B}\mathbf{C}_{cmI}\mathbf{u}_{cm}
\end{aligned}
$$
$$(7)$$

Note that the matrix $\mathbf{C}_{cmI}$ used to transform the inputs is not equal to the matrix $\mathbf{C}_{cm}$ used to transform the states. It contains similar elements, but the size must match the number of the inputs $\mathbf{u}$ rather than the number of states $\mathbf{x}$.

We can now write a Coleman form of equation (4):

$$\mathbf{y}_{cm} = \mathbf{C}_{cmO}^{-1}\mathbf{C}\mathbf{C}_{cm}\mathbf{x}_{cm} + \mathbf{C}_{cmO}^{-1}\mathbf{D}\mathbf{C}_{cmI}\mathbf{u}_{cm} \quad (8)$$

where $\mathbf{C}_{cmO}$ is used as a transform for the outputs.

So far, these equations hold for *any* transformation, as long as the inverse of the transformation and its time derivative exist.

A.2 Applying Coleman transformation with a constant rotor speed

Now lets have a look at what happens when we employ the Coleman transformation for a set of 3 states that are spaced 120 degrees apart on a circle:

$$
\begin{pmatrix} x_{1,cm} \\ x_{2,cm} \\ x_{3,cm} \end{pmatrix} = \mathbf{C}_{cm}^{-1} \begin{pmatrix} x_1 \\ x_2 \\ x_3 \end{pmatrix}
$$

---

[3]The inverse is due to the definition of the Coleman matrix

where:

$$\mathbf{C}_{cm} = \begin{bmatrix} 1 & \sin\psi_1 & \cos\psi_1 \\ 1 & \sin\psi_2 & \cos\psi_2 \\ 1 & \sin\psi_3 & \cos\psi_3 \end{bmatrix} \tag{9}$$

Here, the angles ψ are the angle of each blade with respect to the vertical. That means that as the wind turbine rotates, these values vary; they are time-varying. For the 3 blades turbine:

$$\psi_1 = \alpha, \psi_2 = \alpha + 120°, \psi_3 = \alpha + 240° \tag{10}$$

where α is the azimuth.

The inverse of the Coleman matrix is simply:

$$\mathbf{C}_{cm}^{-1} = \begin{bmatrix} \frac{1}{3} & \frac{1}{3} & \frac{1}{3} \\ \frac{2}{3}\sin\psi_1 & \frac{2}{3}\sin\psi_2 & \frac{2}{3}\sin\psi_3 \\ \frac{2}{3}\cos\psi_1 & \frac{2}{3}\sin\psi_2 & \frac{2}{3}\sin\psi_3 \end{bmatrix} \tag{11}$$

Now we want to apply these matrices to all the states and obtain the correct matrices to apply in equations 7 and 8

Each filter can be defined by their own set of state-space equations:

$$\dot{\mathbf{x}}_{b1} = \mathbf{A}_{b1}\mathbf{x}_{b1} + \mathbf{B}\mathbf{u}_{b1} \tag{12}$$
$$\mathbf{y}_{b1} = \mathbf{C}_{b1}\mathbf{x}_{b1} + \mathbf{D}_{b1}\mathbf{u}_{b1} \tag{13}$$

with

$$\mathbf{x}_{b1} = \begin{pmatrix} x_{1b1} \\ x_{2b1} \\ x_{3b1} \\ \vdots \end{pmatrix}$$

and:

$$\mathbf{A}_{b1} = \begin{bmatrix} a_{1,1b1} & a_{1,2b1} & a_{1,3b1} \\ a_{2,1b1} & a_{2,2b1} & a_{2,3b1} & \cdots \\ a_{3,1b1} & a_{3,2b1} & a_{3,3b1} \\ & \vdots & & \ddots \end{bmatrix}$$

We will organise the states in groups of 3, i.e.:

$$\begin{pmatrix} x_{1b1} \\ x_{1b2} \\ x_{1b3} \\ x_{2b1} \\ x_{2b2} \\ x_{2b3} \\ x_{3b1} \\ x_{3b2} \\ x_{3b3} \\ \vdots \end{pmatrix}$$

which means that:

$$\mathbf{A} = \begin{bmatrix} a_{1,1b1} & 0 & 0 & a_{1,2b1} & 0 & 0 \\ 0 & a_{1,1b2} & 0 & 0 & a_{1,2b2} & 0 \\ 0 & 0 & a_{1,1b3} & 0 & 0 & a_{1,2b3} \cdots \\ a_{2,1b1} & 0 & 0 & a_{2,2b1} & 0 & 0 \\ 0 & a_{2,1b2} & 0 & 0 & a_{2,2b2} & 0 \\ 0 & 0 & a_{2,1b3} & 0 & 0 & a_{2,2b3} \\ & & \vdots & & & & \ddots \end{bmatrix} \tag{14}$$

That means that the transform matrix looks like:

$$\mathbf{C}_{cm,big} = \begin{bmatrix} \mathbf{C}_{cm} & 0 & 0 \\ 0 & \mathbf{C}_{cm} & 0 & \cdots \\ 0 & 0 & \mathbf{C}_{cm} \\ & \vdots & & \ddots \end{bmatrix} \tag{15}$$

And for the inverse:

$$\mathbf{C}_{cm,big}^{-1} = \begin{bmatrix} \mathbf{C}_{cm}^{-1} & 0 & 0 \\ 0 & \mathbf{C}_{cm}^{-1} & 0 & \cdots \\ 0 & 0 & \mathbf{C}_{cm}^{-1} \\ & \vdots & & \ddots \end{bmatrix} \tag{16}$$

We are almost, there we just need the time derivative of this function, we will assume that $\alpha = \omega t$

$$\mathbf{C}_{cm,big}^{-\dot{1}} = \begin{bmatrix} \dot{\mathbf{C}}_{cm}^{-1} & 0 & 0 \\ 0 & \dot{\mathbf{C}}_{cm}^{-1} & 0 & \cdots \\ 0 & 0 & \dot{\mathbf{C}}_{cm}^{-1} \\ & \vdots & & \ddots \end{bmatrix} \tag{17}$$

where:

$$\dot{\mathbf{C}}_{cm}^{-1} = \begin{bmatrix} 0 & 0 & 0 \\ \frac{2}{3}\omega\cos\psi_1 & \frac{2}{3}\omega\cos\psi_2 & \frac{2}{3}\omega\cos\psi_3 \\ \frac{2}{3}\omega\sin\psi_1 & \frac{2}{3}\omega\sin\psi_2 & \frac{2}{3}\omega\sin\psi_3 \end{bmatrix} \tag{18}$$

So now we can combine these with equation (7). Lets have a look how it this works out for the multiplication $\mathbf{C}_{cm}^{-1}\mathbf{A}\mathbf{C}_{cm}$.

Due to the structure of $\mathbf{C}_{cm}^{-1}$ and $\mathbf{C}_{cm}$ the top left corner of the resulting matrix is:

$$\mathbf{C}_{cm}^{-1} \begin{bmatrix} a_{1,1b1} & 0 & 0 \\ 0 & a_{1,1b2} & 0 \\ 0 & 0 & a_{1,1b3} \end{bmatrix} \mathbf{C}_{cm} \tag{19}$$

If we assume that the filters are isotropic (the same on each blade) that means: $a_{1,1b1} = a_{1,1b2} = a_{1,1b3} = a_{1,1}$ and equation (19) simplifies to:

$$a_{1,1}\mathbf{C}_{cm}^{-1}\begin{bmatrix}1 & 0 & 0\\0 & 1 & 0\\0 & 0 & 1\end{bmatrix}\mathbf{C}_{cm}$$

$$= a_{1,1}\mathbf{C}_{cm}^{-1}\mathbf{C}_{cm}$$

$$= a_{1,1}\begin{bmatrix}1 & 0 & 0\\0 & 1 & 0\\0 & 0 & 1\end{bmatrix} \tag{20}$$

This is equal to the original matrix in equation (14). In fact one can show that due to the fact that the filters are equal, equations 7 and 8 simplify to:

$$\dot{\mathbf{x}}_{cm} = \left(\left(\dot{\overline{\mathbf{C}_{cm}^{-1}}}\right)\mathbf{C}_{cm} + \mathbf{A}\right)\mathbf{x}_{cm} + \mathbf{B}\mathbf{u}_{cm} \tag{21}$$

$$\mathbf{y}_{cm} = \mathbf{C}\mathbf{x}_{cm} + \mathbf{D}\mathbf{u}_{cm} \tag{22}$$

Remains the part $\left(\dot{\overline{\mathbf{C}_{cm}^{-1}}}\right)\mathbf{C}_{cm}$. Lets examine the top left part of this multiplication:

$$\begin{bmatrix}0 & 0 & 0\\\frac{2}{3}\omega\cos\psi_1 & \frac{2}{3}\omega\cos\psi_2 & \frac{2}{3}\omega\cos\psi_3\\\frac{2}{3}\omega\sin\psi_1 & \frac{2}{3}\omega\sin\psi_2 & \frac{2}{3}\omega\sin\psi_3\end{bmatrix}\begin{bmatrix}1 & \sin\psi_1 & \cos\psi_1\\1 & \sin\psi_2 & \cos\psi_2\\1 & \sin\psi_3 & \cos\psi_3\end{bmatrix}$$

$$= \begin{bmatrix}0 & 0 & 0\\0 & 0 & \omega\\0 & -\omega & 0\end{bmatrix} \tag{23}$$

These items only occur for the 'on-diagonal' elements. Thus, if we wish to write equation (21) as:

$$\dot{\mathbf{x}}_{cm} = \mathbf{A}_{cm}\mathbf{x}_{cm} + \mathbf{B}\mathbf{u}_{cm} \tag{24}$$

then the matrix $\mathbf{A}_{cm}$:

$$\mathbf{A}_{cm} = \begin{bmatrix}a_{1,1} & 0 & 0 & a_{1,2} & 0 & 0 & \\0 & a_{1,1} & \omega & 0 & a_{1,2} & 0 & \\0 & -\omega & a_{1,1} & 0 & 0 & a_{1,2} & \cdots\\a_{2,1} & 0 & 0 & a_{2,2} & 0 & 0 & \\0 & a_{2,1} & 0 & 0 & a_{2,2} & \omega & \\0 & 0 & a_{2,1} & 0 & -\omega & a_{2,2} & \\ & & \vdots & & & & \ddots\end{bmatrix} \tag{25}$$

	DEQL (MNm)	Reduction	RMS (Blade pitch velocity)	Reduction[2]	RMS (Profile pitch velocity)
11 m/s, nonlinear baseline control					
baseline	6.73	-	0.382	65.6%	0
IPC	6.38	5.2%	1.11	-	0
mmDBC	5.36	20.4%	0.369	66.7%	2.98
mmDBC + IPC	5.32	21.0%	0.531	52.2%	2.59
Skyhook 2p	5.43	19.3%	0.393	64.6%	3.64
Skyhook 2p + IPC	5.22	23.4%	1.08	2.7%	3.58
15 m/s, linearised baseline control					
baseline	9.40	-	0.248	85.6%	0
IPC	6.86	27.0%	1.72	-	0
mmDBC	5.66	39.8%	0.239	86.1%	3.40
mmDBC + IPC	5.41	42.4%	0.925	46.2%	3.47
Skyhook 2p	6.21	33.9%	0.249	85.5%	5.88
Skyhook 2p + IPC	5.03	46.4%	1.60	7.0%	5.68
20 m/s, linearised baseline control					
baseline	11.0	-	0.165	91.0%	0
IPC	8.88	19.3%	1.84	-	0
mmDBC	6.79	38.3%	0.157	91.5%	3.47
mmDBC + IPC	6.63	39.7%	1.02	44.6%	3.40
Skyhook 2p	6.82	38.0%	0.165	91.0%	6.97
Skyhook 2p + IPC	5.79	47.4%	1.68	8.7%	6.80

Table 2: Effect of control strategy on damage equivalent blade root moments and control effort in 500 second simulations

	DEQL (Tower fore-aft)	Reduction	DEQL (Tower sideways)	Reduction
11 m/s, nonlinear baseline control				
baseline	7.27e-3	-	1.22e-3	-
IPC	7.49e-3	-3.0%	1.25e-3	-2.4%
mmDBC	6.75e-3	7.2%	1.40e-3	-14.0%
mmDBC + IPC	6.68e-3	8.2%	1.29e-3	-5.5%
Skyhook 2p	6.23e-3	14.3%	1.20e-3	2.1%
Skyhook 2p + IPC	6.34e-3	12.7%	1.18e-3	3.9%
15 m/s, linearised baseline control				
baseline	5.59e-3	-	3.60e-3	-
IPC	5.60e-3	0.9%	3.45e-3	4.4%
mmDBC	5.85e-3	2.8%	4.34e-3	-20.3%
mmDBC + IPC	5.91e-3	3.0%	5.05e-3	-40.2%
Skyhook 2p	3.33e-3	26.4%	3.43e-3	4.8%
Skyhook 2p + IPC	3.34e-3	26.9%	3.42e-3	5.11%
20 m/s, linearised baseline control				
baseline	7.73e-3	-	4.69e-3	-
IPC	7.75e-3	0.3%	4.64e-3	-0.9%
mmDBC	8.41e-3	-8.8%	6.51e-3	-38.9%
mmDBC + IPC	8.84e-3	-14.4%	6.48e-3	-38.3%
Skyhook 2p	5.34e-3	31.0%	3.63e-3	22.6%
Skyhook 2p + IPC	5.31e-3	31.3%	3.56e-3	24.1%

Table 3: Effect of control strategy on tower top 'design equivalent translation'